IEEE Access
Multidisciplinary : Rapid Review : Open Access Journal

Received March 26, 2020, accepted April 4, 2020, date of publication April 14, 2020, date of current version April 30, 2020.

Digital Object Identifier 10.1109/ACCESS.2020.2987825

Argon Precursor Ion Implantation Used to Activate Boron Atoms in Silicon at Low Temperatures

TOSHIYUKI SAMESHIMA[1], TOMOKAZU NAGAO[2], ERIKA SEKIGUCHI[1], AND MASAHIKO HASUMI[1]
[1]Graduate School of Engineering, Tokyo University of Agriculture and Technology, Tokyo 184-8588, Japan
[2]Nissin Ion Equipment Company, Ltd., Kyoto 528-0068, Japan

Corresponding author: Toshiyuki Sameshima (tsamesim@cc.tuat.ac.jp)

This work was supported by the collabolation budget given by NISSIN ION.

ABSTRACT The two-step implantation of argon precursor ion (Ar^+) followed by boron ion (B^+) in single crystalline silicon at room temperature is discussed to activate boron implanted region by post heating at 300 followed by 400°C. The implantation of Ar^+ at a dose of 6.0×10^{13} cm^{-2} at 70 keV with a projected range R_p(Ar) of 80 nm followed by B^+ at 1.0×10^{15} cm^{-2} and 15 keV with R_p(B) of 62 nm caused crystalline disordered states with the effective disordered amorphous depth A_{eff} of 32 nm, while the post heating of 300°C for 90 min followed by 400°C for 30 min markedly decreased A_{eff} to 1.8 nm. The effective recrystallization by the post heating promoted activation of doped region associated with decrease in the sheet resistivity to 189 Ω/sq by the post heating. The activation ratio was estimated as 0.33 under the assumption of a hole mobility of 50 cm^2/Vs in the boron implanted region.

INDEX TERMS Activation, carrier density, carrier lifetime, defect, low temperature.

I. INTRODUCTION

Low temperature processing is important to achieve the low thermal budget for fabricating semiconductor devices. It realizes a low tact time of device fabrication and low-cost production. Especially, the low temperature fabrication technology is important to fabricate polycrystalline silicon thin film transistors (poly-Si TFTs), photo sensors, and solar cells on low thermal proof substrates, for example, glass and plastic substrates [1]–[5]. Ion implantation is an essential technology for incorporating dopant atoms in semiconductor. It has established itself as a tool for forming the source/drain regions for fabricating transistors and the pn junction for photo sensors. However, the activation of dopant atoms at a low temperature has been a serious problem to apply the ion implantation technology to device fabrication processing at a low temperature. In general, heating at temperature higher than 600°C is required owing to the large activation energy for moving dopant atoms from the interstitial sites to the lattice sites or giving thermal energy enough to recrystallize disordered silicon state caused by high energy ion implantation [6]–[10]. Reduction of the activation energy and effective recrystallization of disordered states are necessary to realize the activation of implanted region at a low temperature.

This paper discusses a two-step-ion implantation of argon precursor ion (Ar^+) followed by boron dopant ion (B^+) implantations to achieve dopant activation and carrier generation at a low temperature by post heating at 300 followed by 400°C. Decrease in the sheet resistivity and increase in the dopant activation ratio are demonstrated with association of Ar^+ precursor ion implantation. This paper demonstrates that disordered states caused by the two-step implantation is effective for dopant activation at a low temperature.

The associate editor coordinating the review of this manuscript and approving it for publication was Kuan Chee.

II. MODEL AND EXPERIMENTAL PROCEDURE

Ar^+ is selected as the precursor implantation to form silicon disordered states associated with silicon bonding distortion, which will decrease the average bonding energy of the silicon lattice. Decreasing the average bonding energy is an advantage for the boron atoms implanted in the interstitial sites to move in the silicon lattice sites by post heating at a low temperature. It will be a practical advantage that Ar^+ implantation easily causes silicon disordered states with a low dose because Ar atom is heavier than silicon atom. It will be also important to keep crystalline states partially as the crystalline

This work is licensed under a Creative Commons Attribution 4.0 License. For more information, see https://creativecommons.org/licenses/by/4.0/

nucleation site in the Ar^+ precursor implanted regions by selecting the Ar^+ dose to recrystallize the disordered states by the post heating at low temperatures. From our concern of poly-Si TFTs whose source and drain regions are fabricated by ion implantation with dopant species of phosphorus and boron, with their dose of about 1×10^{15} cm^{-2}, and projected range from 50 to 100 nm in general, boron implantation was investigated in this paper under the conditions of a dose of 1.0×10^{15} cm^{-2}. We used the heating temperatures of 300 and 400°C, which are the conventional heating temperatures for activating the dopant atoms in the source and drain regions for poly-Si TFTs. After our preliminary reports [11], we set following experimental procedures to precisely investigate the coherent relations between activation of dopant atoms and disordered states.

For investigating an appropriate dose of Ar^+ precursor, we set it ranging from 1.0×10^{13} to 5.0×10^{14} cm^{-2} under the implantation conditions of an acceleration energy of 70 keV at RT to n-type CZ single crystalline silicon substrates with a thickness of 500 μm and a resistivity higher than 1500 Ωcm. Calculation with the program of transport of ions in matter (TRIM [12]) resulted in a projected range R_p(Ar) of 80 nm. B^+ ions were subsequently implanted at RT. The acceleration energy, R_p(B), and dose were 20 keV, 80 nm, and 1.0×10^{15} cm^{-2}, respectively. Ar^+ followed by B^+ implantations were carried out to the top and rear silicon surfaces. The total dose was therefore two times of that given above. The samples were then heated at 300°C for 90 min in the air atmosphere. After investigation of changes in crystalline and electrical properties of implanted regions, the samples were subsequently heated at 400°C for 30 min in the air atmosphere.

For the second experiment, the relation between R_p(Ar) and R_p(B) was investigated by changing the acceleration energy of the second 1.0×10^{15}-cm^{-2}-B^+ implantation at RT between 5 and 50 keV. R_p(B) ranged from 23 to 175 nm. Ar^+ precursor implantation was set at 70 keV and 6.0×10^{13} cm^{-2}, and RT. Ar^+ precursor implantation followed by B^+ implantations were carried out to the top and rear silicon surfaces. The samples were then heated by 300°C for 90 min followed by 400°C for 30 min in the air atmosphere.

In order to analyze the crystalline state in the ion implanted region in the process steps of ion implantation and post heating, the non-destructive measurement of optical reflectivity spectra was used. The optical reflectivity spectra of the silicon surfaces were measured for wavelength ranging from 250 to 1000 nm using a conventional optical spectrometer. The complex refractive index sensitively changes associated with disordered bonding states caused by ion implantation. The surface structure with different complex refractive indices from that of single crystalline silicon can change the shape of optical reflectivity spectrum. Optical interference effect also occurs because the depths of ion implantation were similar or lower than the wavelengths of light. The experimental optical reflectivity spectra were analyzed using a home-made numerical calculation program developed with the optical interference effect and the effective dielectric media approximation with a model of seven silicon layered structure with different crystalline fraction X and thickness d formed on single crystalline silicon substrate [13], [14]. The crystalline fraction X_i at i^{th} layer with a thickness d_i is determined as a coefficient when the effective complex refractive index n_i at i^{th} layer is assumed to be given by the linear combination of complex refractive indices of crystalline silicon n_c and amorphous silicon n_a as,

$$n_i = X_i n_c + (1 - X_i) n_a. \tag{1}$$

The optical absorption coefficient is very high on the order of 10^6 cm^{-1} for wavelength lower than 350 nm. The optical reflectivity in the ultraviolet region gives information of the effective complex refractive index in the 10-nm-deep surface region. The optical absorption coefficient decreases as the wavelength increases from 350 nm because of the silicon indirect band structure. The optical reflectivity for long wavelength therefore includes information of the effective complex refractive index of a deep region. X in the shallow surface region is therefore determined by fitting the calculated optical reflectivity to the experimental optical reflectivity in the ultraviolet region Then X values in deeper regions was analyzed using the optical reflectivity spectra for longer wavelength to obtain the in-depth X_i profile. The fitting was conducted with the least squares method by changing X_i and d_i for the seven layers until the squared root of the sum of squared residuals between experimental reflectivity r_e (%) and calculated reflectivity r_c (%) integrated from 250 to 1000 nm S was lower than 1%, which was equivalent to 1% difference between experimental and calculated reflectivity values in average between 250 and 1000 nm, as,

$$S = \sqrt{\frac{\int_{250}^{1000} (r_e - r_c)^2 \, d\lambda}{750}} < 1, \tag{2}$$

where λ is the wavelength. Figure 1 shows the demonstration of (a) experimental optical reflectivity spectra of single crystalline silicon (black solid curve), as-ion implanted Ar^+ at 70 keV and 6.0×10^{13} cm^{-2} followed by B^+ at 20 keV and 1.0×10^{15} cm^{-2} (red solid curve), and calculated spectrum fitted to the experimental spectrum of the as-implanted sample (red dashed curve), (b) the in-depth crystalline fraction X profile obtained by the spectral fitting shown in Fig. 1(a), and (c) a bright field image of transmission electron microscope (TEM) of the as-implanted sample. The spectrum of the single crystalline silicon shows the two large peaks of E_2 and E_1 caused by the large joint density of states in the Brillouin zone of crystalline silicon appeared at 275 and 340 nm and monotonously decrease in the optical reflectivity according to monotonous decreases in the refractive index and extinction coefficient as the wavelength increases from 340 nm. The two-step implantation of Ar^+ and B^+ slightly decreased the optical reflectivity in the ultraviolet region and waved the spectrum shape in visible and infrared regions shown by the red curve. The almost same spectral shapes were observed at different places of the sample within a detection limit of the

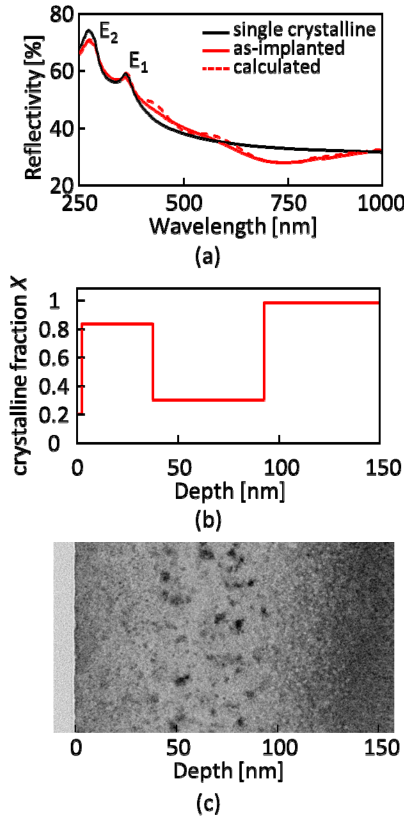

FIGURE 1. (a) Experimental optical reflectivity spectra of single crystalline silicon, as-ion implanted Ar^+ at 70 keV and 6.0×10^{13} cm^{-2} followed by B^+ at 20 keV and 1.0×10^{15} cm^{-2}, and calculated spectrum, (b) the in-depth crystalline fraction X profile obtained by the spectral fitting, and (c) a bright field image of transmission electron microscope (TEM) of the as-implanted sample.

spectrometer of 0.5%. The calculated spectrum (red dashed curve) well fitted the experimental spectrum with a S value of 0.86%. The fitting resulted in X as a function of depth as shown in Fig.1 (b). X in the surface region was decreased by the ion implantation. Especially X decreased to 0.35 in the depth between 35 and 90 nm. this indicates that a buried disordered region was formed by the ion implantation. The image of TEM shows many dark spots indicating disordered sites. The dark spots concentrated at the almost coincident depth with low X. The results of Figs. 1(a) to (c) indicate the capability of the optical reflectivity spectrum analysis for non-destructively investigating the disordered states caused by ion implantation.

We also introduced the effective disordered amorphous depth A_{eff} as an index of disorder states formed in silicon substrate by integration of the product of 1-X_i and d_i at i^{th} layer as,

$$A_{eff} = \sum_i (1 - X_i) \times d_i. \quad (3)$$

To investigate the electrical conductivity and carrier lifetime, we used a 9.35-GHz-microwave-transmittance measurement system [15], [16]. The system had waveguide tubes, which had a narrow gap where a sample was placed. Continuous-wave (CW) 635 nm laser diode (LD) light with a penetration depth of 2.7 μm was introduced into the waveguide tubes. The light intensities were set at 0.74 mW/cm^2 on the sample surface for 635 nm lights. In a dark field, the microwave was absorbed by free carrier in the silicon substrate by so-called Drude effect [17]. The microwave transmittance T_d was analyzed with a finite-element numerical calculation program made with a Fresnel-type microwave interference effect and the free carrier absorption to estimate the sheet resistivity, which was obtained by fitting the calculated T_d to the experimental T_d. The microwave transmittance under the light illumination of the ion-implanted surface T_p was also measured to obtain the photo-induced minority carrier effective lifetime τ_{eff}. τ_{eff} was analyzed by the numerical program of carrier diffusion and annihilation to estimate the carrier recombination velocity at the implanted surfaces [18].

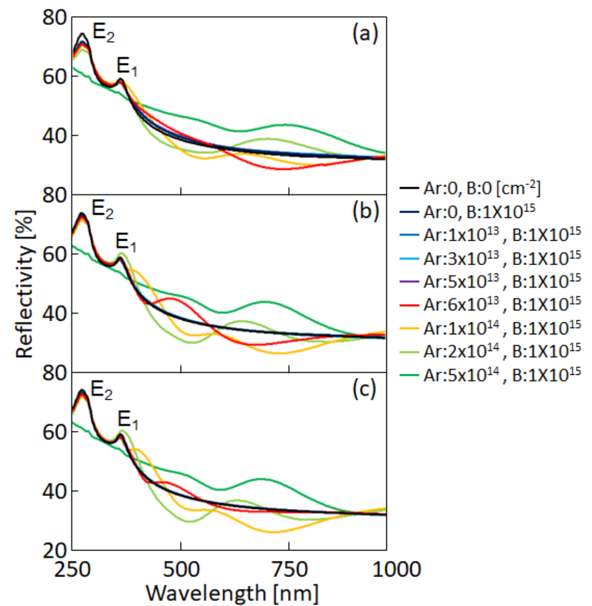

FIGURE 2. Optical reflectivity spectra of the samples (a) as-implanted with Ar^+ with the dose ranging from 0 to 5.0×10^{14} cm^{-2} at 70 keV at RT followed by B^+ with the dose of 1.0×10^{15} cm^{-2} at 20 keV at RT, (b) heated at 300°C for 90 min, and (c) subsequently heated at 400°C for 30 min.

III. RESULTS AND DISCUSSIONS

Figure 2 shows the optical reflectivity spectra of the samples (a) as-implanted with Ar^+ with the dose ranging from 0 to 5.0×10^{14} cm^{-2} at 70 keV at RT followed by B^+ with the dose of 1.0×10^{15} cm^{-2} at 20 keV at RT, (b) heated at 300°C for 90 min, and (c) subsequently heated at 400°C for 30 min. The optical reflectivity spectra of the single crystalline silicon sample were also plotted by black solid curve in each graph. The single B^+ implantation slightly decreased the optical reflectivity spectra in the ultraviolet region. The E_1 and E_2 peaks were slightly decreased. This means that disordered state was formed in the shallow surface region.

Ar^+ implantation changed the optical reflectivity spectra. The E_1 and E_2 peaks further decreased as the dose of Ar^+ implantation increased to 2.0×10^{14} cm^{-2}, although the spectrum had no E_1 and E_2 peaks for the Ar^+ dose of 5.0×10^{14} cm^{-2} as shown in Fig. 2(a). It shows that the disordered state increased in the silicon surface regions as the Ar^+ dose increased, while the crystalline state still remained at the surface region for Ar^+ dose lower than or equal to 2.0×10^{14} cm^{-2}. On the other hand, the silicon surface region was completely amorphized by 5.0×10^{14} cm^{-2}-Ar^+ implantation. Marked spectral fringes appeared in visible and near infrared region for Ar^+ doses between 6.0×10^{13} and 5.0×10^{14} cm^{-2}. High optical interference occurred owing to the formation of thick regions with refractive indices different from that of single crystalline silicon by Ar^+ implantation. These spectra indicate that substantial disordered regions were formed by the two-step implantation.

Post heating at 300°C for 90 min increased the heights of the E_1 and E_2 peaks for Ar^+ dose lower than or equal to 2.0×10^{14} cm^{-2}, as shown in Fig. 2(b). This indicates the crystalline fraction X increased at the silicon surface region by the post heating. However, there were still no E_1 and E_2 peaks for the Ar^+ dose of 5.0×10^{14} cm^{-2}. The amorphous region was not crystallized by the heating at 300°C. The spectral fringes were still observed for Ar^+ doses between 6.0×10^{13} and 5.0×10^{14} cm^{-2}. Internal disordered states still remained. Post heating at 400°C for 30 min further increased the heights of the E_1 and E_2 peaks close to those of single crystalline for Ar^+ dose lower than or equal to 2.0×10^{14} cm^{-2}, as shown in Fig. 2(c). Disordered region was reduced at the silicon surface region by the post heating. However, there were still no E_1 and E_2 peaks appeared for the Ar^+ dose of 5.0×10^{14} cm^{-2}. Heating at 400°C was not sufficient to recrystallize the amorphous region formed by Ar^+ implantation at 5.0×10^{14} cm^{-2}. The amplitude of the spectral fringe for the Ar^+ dose of 6.0×10^{13} cm^{-2} was markedly decreased by the heating at 400°C. This indicates that disordered states were reduced and the recrystallization was proceeded by the post heating. On the other hand, Large spectral fringes were still observed for Ar^+ doses between 1.0×10^{14} and 5.0×10^{14} cm^{-2}. Internal disordered states still remained.

Figure 3 shows the in-depth profiles of X obtained by analyzing the optical reflectivity spectra of the samples (a) as-implanted with Ar^+ with the dose ranging from 0 to 5.0×10^{14} cm^{-2} at 70 keV at RT followed by B^+ with the dose of 1.0×10^{15} cm^{-2} at 20 keV at RT, (b) heated at 300°C for 90 min, and (c) subsequently heated at 400°C for 30 min. X slightly decreased to 0.72 in the surface 10 nm deep region as Ar^+ dose increased to 5.0×10^{13} cm^{-2}. On the other hand, X markedly decreased in the wide depth region as the dose of Ar^+ increased from 6.0×10^{13} cm^{-2}, as shown in Fig. 3(a). The minimum X decreased from 0.3 to 0 as the dose of Ar^+ increased from 6.0×10^{13} to 5.0×10^{14} cm^{-2}. Substantial defects were formed in Ar^+ implantation region with high doses. Heating at 300°C for 90 min increased X in

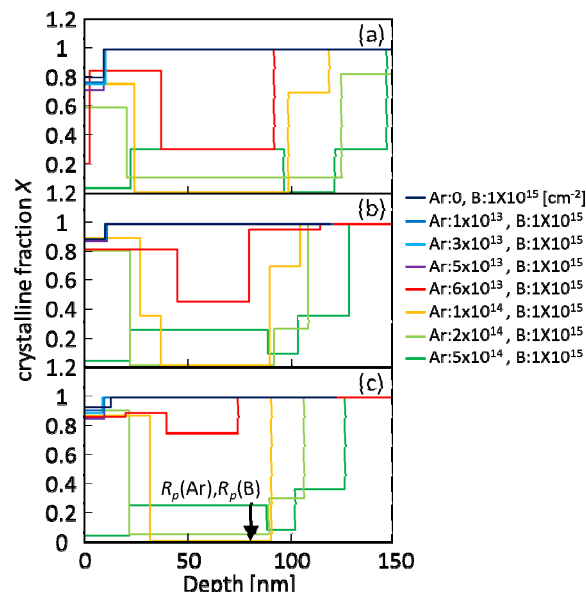

FIGURE 3. In-depth profiles of X, (a) as-implanted with Ar^+ with the dose ranging from 0 to 5.0×10^{14} cm^{-2} at 70 keV at RT followed by B^+ with the dose of 1.0×10^{15} cm^{-2} at 20 keV at RT, (b) heated at 300°C for 90 min, and (c) subsequently heated at 400°C for 30 min. R_p(Ar) and R_p(B) of 80 nm are indicated by arrows on the depth axis.

the cases of low Ar^+ doses, as shown in Fig. 3(b). Especially X markedly increased from 0.3 to 0.45 for the depth between 40 and 80 nm in the case of Ar^+ dose of 6.0×10^{13} cm^{-2}. The disordered state was well recrystallized by heating at 300°C for 90 min. On the other hand, the low X hardly changed for the Ar^+ doses higher than 1.0×10^{14} cm^{-2}. High disordered region was not recrystallized well by heating at 300°C for 90 min. For the subsequent heating at 400°C for 30 min further increased X to 0.75 for the depth between 40 and 75 nm in the case of Ar^+ dose of 6.0×10^{13} cm^{-2}. On the other hand, the low X hardly changed for the Ar^+ doses higher than 1.0×10^{14} cm^{-2}.

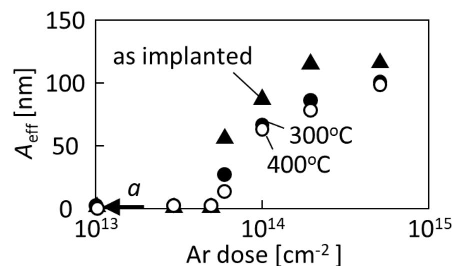

FIGURE 4. A_{eff} obtained by eq. 3 with X shown in Fig. 3 as a function of the Ar^+ dose for the samples as-two-step implanted (solid triangles), heated at 300°C for 90 min (solid circles), and subsequently heated at 400°C for 30 min (open circles). The arrow a presents A_{eff} of 1.8 nm for the case of single B^+ implantation at 1.0×10^{15} cm^{-2} and 20 keV.

Figure 4 shows A_{eff} defined by eq. 3 with X shown in Fig. 3 as a function of the Ar^+ dose for the samples as-two-step implanted (solid triangles), heated at 300°C for 90 min (solid circles), and subsequently heated at 400°C for

30 min (open circles). A_{eff} for the sample with the single B^+ as implantation was also presented by an arrow *a* in Fig. 4. For the Ar^+ dose lower than or equal to 5.0×10^{13} cm^{-2}, A_{eff} had a low value about 2.5 nm, which was similar to 1.8 nm in the case of the single B^+ implantation for as-implanted samples. A_{eff} markedly increased from 55 to 116 nm as the Ar^+ dose increased from 6.0×10^{13} to 5.0×10^{14} cm^{-2}. This analysis indicates that the threshold dose of Ar^+ was 5.0×10^{13} cm^{-2} to form substantial disordered amorphous region. The results of Fig. 3 also show that the dose of Ar^+ of 1.0×10^{14} cm^{-2} or above resulted in a complete amorphous layer. The condition of Ar^+ dose of 6.0×10^{13} cm^{-2} formed the surface 100 nm deep region with the coexistence of disordered states and crystalline states. The heating at 300°C for 90 min decreased A_{eff}. For the Ar^+ dose lower than or equal to 5.0×10^{13} cm^{-2}, A_{eff} had a low value about 1.3 nm, which was similar to 1.1 nm in the case of the single B^+ implantation. A_{eff} markedly decreased from 55 to 29 nm in the case of Ar^+ dose of 6.0×10^{13} cm^{-2}. On the other hand, A_{eff} had kept high value under the heating at 300°C for 90 min for Ar^+ dose ranging from 1.0×10^{14} to 5.0×10^{14} cm^{-2}. The subsequent heating at 400°C for 30 min further decreased A_{eff}. Especially, A_{eff} markedly decreased from 13 nm in the case of Ar^+ dose of 6.0×10^{13} cm^{-2}. On the other hand, A_{eff} had kept high value under the heating at 400°C for 30 min for Ar^+ dose ranging from 1.0×10^{14} to 5.0×10^{14} cm^{-2}.

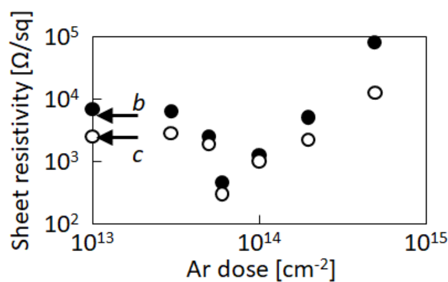

FIGURE 5. Sheet resistivity as a function of the Ar^+ dose for the two-step-implanted samples heated at 300°C for 90 min (solid circles), and subsequently heated at 400°C for 30 min (open circles). The arrows of *b* and *c* present the sheet resistivity for the cases of single B^+ implantation at 1.0×10^{15} cm^{-2} and 20 keV followed by post heating 300°C for 90 min and 400°C for 30 min, respectively.

Figure 5 shows the sheet resistivity as a function of the Ar^+ dose for the two-step-implanted samples heated at 300°C for 90 min (solid circles), and subsequently heated at 400°C for 30 min (open circles). Although the sheet resistivity was higher than the measurement limit of 80000 Ω/sq for all as-implanted samples, the post heating at 300°C for 90 min decreased the sheet resistivity which strongly depended on the Ar^+ dose, as shown in Fig. 5. While the sheet resistivity was high of about 6600 Ω/sq for the Ar^+ doses up to 3.0×10^{13} cm^{-2}, which was similar value to 5500 Ω/sq for single B^+ implantation sample, as shown by an arrow *b* in Fig. 5, it markedly decreased to 444 Ω/sq as the Ar^+ dose increased to 6.0×10^{13} cm^{-2}. On the other hand, the sheet resistivity increased to very high value above the measurement limit of 80000 Ω/sq as the Ar^+ dose further increased to 5.0×10^{14} cm^{-2}. A resonant phenomenon of decrease in the resistivity as a function of Ar^+ dose was observed. The post heating at 400°C for 30 min further decreased the sheet resistivity, as shown by open circles in Fig. 5. In similar manner to the case of 300°C heating case, the sheet resistivity was high of about 2500 Ω/sq for the Ar^+ doses up to 3.0×10^{13} cm^{-2}, which was similar value to 2400 Ω/sq for single B^+ implantation sample, as shown by an arrow *c*. It markedly decreased to 302 Ω/sq as the Ar^+ dose increased to 6.0×10^{13} cm^{-2}. Then the sheet resistivity increased to 10000 Ω/sq as the Ar^+ dose further increased to 5.0×10^{14} cm^{-2}.

The results of Fig. 5 revealed that there was a resonant value of Ar^+ dose of 6.0×10^{13} cm^{-2} for activating boron doped region implanted with 1.0×10^{15} cm^{-2} B^+ in the case of the same value of R_P(Ar) and R_p(B) of 80 nm. The analyses of the crystalline properties shown in Figs. 3 and 4 also suggest that the substantial crystalline disordered state was formed by the Ar^+ precursor implantation at 6.0×10^{13} cm^{-2} and 70 keV with R_p(Ar) of 80 nm followed by B^+ implantation at 1.0×10^{15} cm^{-2} and 20 keV with R_p(B) of 80 nm, and that effective recrystallization was achieved by the post heating at the low temperature of 400°C. The recrystallization probably promoted the resonant decrease in the sheet resistivity as shown in Fig. 5.

Next, the best R_p(B) was researched to the R_P(Ar) of 80 nm for activation of boron implanted region. The two-step implantation was carried out with the conditions of Ar^+ at 6.0×10^{13} cm^{-2} and 70 keV (R_P(Ar) = 80 nm) and B^+ at 1.0×10^{15} cm^{-2} and the acceleration energy ranging from 5 to 50 keV, which gave R_p(B) ranged from 23 to 175 nm. The post heating of 300°C for 90 min followed by 400°C for 30 min was subsequently treated. Figure 6 shows the optical reflectivity spectra of the samples (a) as-implanted with Ar^+ with the dose of 6.0×10^{13} cm^{-2} at 70 keV and RT followed by B^+ with the dose of 1.0×10^{15} cm^{-2} at the acceleration energies ranging from 5 to 50 keV at RT, (b) heated at 300°C for 90 min, and (c) subsequently heated at 400°C for 30 min. The optical reflectivity spectra of the single crystalline silicon sample (before implantation) and single Ar^+ implantation with the dose of 6.0×10^{13} cm^{-2} at 70 keV were also plotted. For as-implanted samples, the optical reflectivity spectrum of single Ar^+ implantation with the dose of 6.0×10^{13} cm^{-2} at 70 keV was almost same as that of single crystalline silicon. This means that single Ar^+ implantation with the dose 6.0×10^{13} cm^{-2} caused small disordered states. On the other hand, subsequent B^+ implantation changed optical reflectivity spectra. In the cases of low acceleration energies of 5 and 10 keV for B^+ implantation, E_1 and E_2 peaks in the ultraviolet region decreased. This indicates that the surface shallow region was disordered. Optical reflectivity spectra showed small spectral fringes in visible and infrared wavelength regions. This suggests that slightly disordered regions were formed in deep regions. In the cases of B^+ acceleration energies from 15 to 35 keV whose projected ranges were

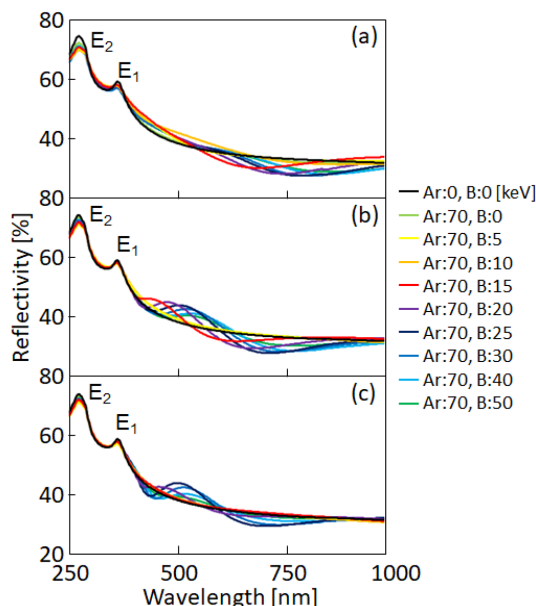

FIGURE 6. Optical reflectivity spectra of the samples (a) as-implanted with Ar^+ with the dose of 6.0×10^{13} cm^{-2} at 70 keV and RT followed by B^+ with the dose of 1.0×10^{15} cm^{-2} at the acceleration energies ranging from 5 to 50 keV at RT, (b) heated at 300°C for 90 min, and (c) subsequently heated at 400°C for 30 min.

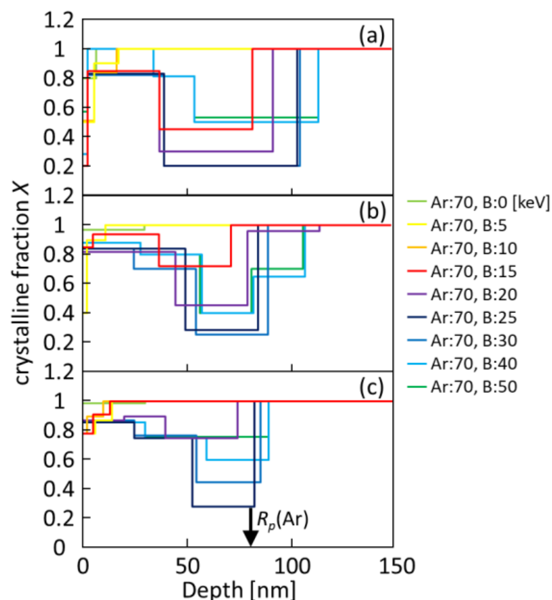

FIGURE 7. In-depth profiles of X of the samples (a) as-implanted with Ar^+ with the dose of 6.0×10^{13} cm^{-2} at 70 keV at RT followed by B^+ with the dose of 1.0×10^{15} cm^{-2} at the acceleration energies ranging from 5 to 50 keV at RT, (b) heated at 300°C for 90 min, and (c) subsequently heated at 400°C for 30 min. R_p(Ar) of 80 nm is indicated by an arrow on the depth axis.

close to that of Ar implantation, optical reflectivity spectra had large spectral fringes in visible and infrared wavelength regions. This means that serious disordered regions were formed in deep regions. The post heating at 300°C for 90 min markedly increased E_1 and E_2 peaks. The disordered states in the surface region was cured by the heat treatment for B^+ implantation. Moreover, the optical interferential fringe was markedly reduced in the case of 5 and 10 keV. The disordered region was effectively reduced. On the other hand, spectral fringes still appeared in visible and infrared ranges in the case of B^+ acceleration energies higher than 15 keV. The disordered region still existed. The subsequent heating at 400°C for 30 min further increased E_1 and E_2 peaks and decreased the amplitudes of the spectral fringes in the visible and infrared region. the crystalline quality was improved by the heat treatment. Especially, the spectral fringes were markedly reduced by the post heating at 400°C in the case of 15 keV. The disordered region was effectively reduced.

Figure 7 shows the in-depth profiles of X obtained by analyzing the optical reflectivity spectra of the samples (a) as-implanted with Ar^+ with the dose of 6.0×10^{13} cm^{-2} at 70 keV and RT followed by B^+ with the dose of 1.0×10^{15} cm^{-2} at the acceleration energies ranging from 5 to 50 keV at RT, (b) heated at 300°C for 90 min, and (c) subsequently heated at 400°C for 30 min. The X in the case of single Ar^+ implantation with the dose of 6.0×10^{13} cm^{-2} at 70 keV were also plotted. X decreased to 0.55 in the surface 5 nm deep region for the single Ar^+ implantation. X slightly decreased in the wide depth ranging 50∼60 nm in the cases of low acceleration energies of 5 and 10 keV for B^+ implantation. X decreased between 0.2 and 0.6 in the depth ranging from 40 to 110 nm in the case of B^+ acceleration energies higher than 10 keV, as shown in Fig. 7(a). Heating at 300°C for 90 min increased X. Especially, in the cases of the acceleration energies of 5 and 10 keV for B^+ implantation, the region with X lower than 1 was limited at the surface region. X also increased from 0.48 to 0.72 in the deep region, in the case of B^+ implantation at 15 keV, as shown Fig. 7(b). The depth width low X was decreased by the heating for every implantation condition. Subsequent heating at 400°C for 30 min further increased X. The region with X lower than 1 was limited at the surface region in the case of B^+ implantation at 15 keV. The region with low X was limited close to R_p(Ar) (=80 nm) for the acceleration energy higher than 20 keV for B^+ implantation. It suggested that the disordered defect region cooperatively formed by implantation of Ar^+ and B^+ atoms with high acceleration energies remained.

Figure 8 shows (a) A_{eff} obtained by eq. 3 with X shown in Fig. 7 as a function of R_p(B) for the samples as-two-step implanted (solid triangles), heated at 300°C for 90 min (solid circles), and subsequently heated at 400°C for 30 min (open circles) and (b) the ratio of A_{eff} for the samples heated at 300°C for 90 min (solid circles), and subsequently heated at 400°C for 30 min (open circles) to A_{eff} as-two-step implanted as a function of R_p(B). The single 6.0×10^{13} cm^{-2} Ar implantation at 70 keV caused small disordered state with A_{eff} of 1.2 nm, as shown by an arrow d in Fig. 8(a). A_{eff} were also low values for R_p(B) of 23 (B^+ acceleration energy of 5 keV) and 42 nm (10 keV). On the other hand, A_{eff} increased

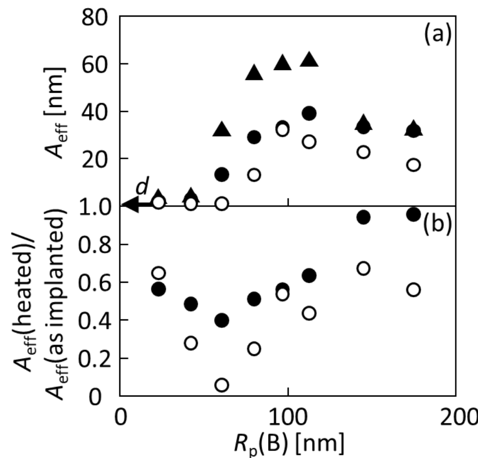

FIGURE 8. **(a) A_{eff} obtained by eq. 3 with X shown in Fig. 7 as a function of R_p(B) for the sample as-two-step implanted (solid triangles), heated at 300°C for 90 min (solid circles), and subsequently heated at 400°C for 30 min (open circles) and (b) the ratio of A_{eff} for the samples heated at 300°C for 90 min (solid circles), and subsequently heated at 400°C for 30 min (open circles) to A_{eff} as-two-step implanted as a function of R_p(B). The arrow d presents an A_{eff} of 1.2 nm caused by single 6.0×10^{13} cm^{-2} Ar^+ implantation at 70 keV.**

from 32 to 61 nm, as R_p(B) increased from 61 (15 keV) to 113 nm (30 keV). When R_p(B) further increased to 175 nm (50 keV), A_{eff} decreased to 38 nm, as shown in Fig. 8(a). This means the implantation of Ar^+ and B^+ cooperatively caused serious disordered states. The post heating at 300°C for 90 min decreased A_{eff}. Especially, in the case of R_p(B) of 61 nm, A_{eff} was decreased from 32 to 12.5 nm by the post heating at 300°C for 90 min. On the other hand, high initial A_{eff} caused by high R_p(B) conditions did not decreased so much. The post heating at 400°C for 30 min further decreased A_{eff}. Especially, in the case of R_p(B) of 61 nm, A_{eff} was marked decreased from 32 to 1.8 nm by the post heating at 400°C for 30 min. On the other hand, high A_{eff} value about 20 nm remained for R_p(B) higher than 96 nm (25 keV), which was higher than R_p(Ar). This indicates that serious defect states, which especially remained after heating, were formed when B atoms traversed the Ar peak concentration region with the high acceleration energies. Figure 8(b) clearly shows that $A_{eff}$was resonantly decreased to 6% of the initial A_{eff} for the sample as implanted at R_p(B) of 61 nm by post heating at 400°C. Figure 7 suggests that decrease in X in the boron doped region to about 0.5 is important to cause recrystallization by the post heating at the low temperature probably because many crystalline sites remained have a role of promotion of recrystallization. The result of Fig. 8 concludes that the disordered states cooperatively formed with Ar^+ and B^+ implantations is effectively recrystallized by post heating at the low temperature under the condition of R_p(B) slight shallower than R_p(Ar).

Figure 9 shows the sheet resistivity as a function of R_p(B) for the 6.0×10^{13} cm^{-2} Ar^+ at 70 keV followed by 1.0×10^{15} cm^{-2} B^+ two-step-implanted samples heated at 300°C for

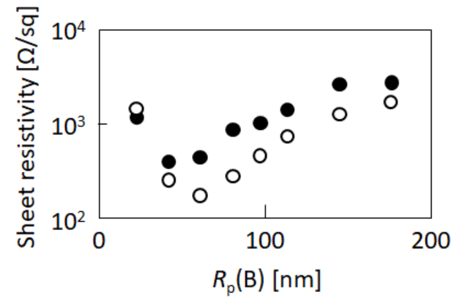

FIGURE 9. **Sheet resistivity as a function of R_p(B) for the 6.0×10^{13} cm^{-2} Ar^+ followed by 1.0×10^{15} cm^{-2} B^+ two-step-implanted samples heated at 300°C for 90 min (solid circles), and subsequently heated at 400°C for 30 min (open circles).**

90 min (solid circles), and subsequently heated at 400°C for 30 min (open circles). Although the sheet resistivity was still high of 1260 Ω/sq when R_p(B) was shallow of 23 nm, it decreased to 392 Ω/sq as R_p(B) increased to 42 nm for sample heating at 300°C for 90 min. This means that the activation of boron atoms is governed by the in-depth distributions of argon and boron atoms. On the other hand, the sheet resistivity increased to a very high value of 2742 Ω/sq as the R_p(B) increased to 175 nm. This indicates that the activation ratio of boron atoms can be low in the case of far deep distribution of the boron atoms from that of argon atoms. The subsequent post heating at 400°C for 30 min further decreased the sheet resistivity. The sheet resistivity decreased to 189 Ω/sq as R_p(B) increased to 61 nm. High activation of boron atoms was achieved when R_p(B) was slightly lower than R_p(Ar) of 80 nm. The sheet resistivity increased to a high value of 1767 Ω/sq as R_p(B) increased to 175 nm as similar behavior of heating at 300°C for 90 min.

The activation ratio P was estimated by assuming a hole mobility μ of 50 cm^2/Vs in the heavily doped condition [19]. P is given as,

$$P = \left(\rho \times \mu \times e \times 2.0 \times 10^{15}\right)^{-1}, \tag{4}$$

where ρ is the sheet resistivity, e is the elemental charge of 1.6×10^{-19} C, and 2.0×10^{15} cm^{-2} is the total boron dose. Figure 10 shows P as a function of R_p(B) with the 6.0×10^{13} cm^{-2} Ar^+ followed by 1.0×10^{15} cm^{-2} B^+ two-step-implanted samples heated at 300°C for 90 min (solid circles), and subsequently heated at 400°C for 30 min (open circles). P increased as R_p(B) increased as shown in Fig. 10. The maximum P was 0.16 at R_p(B) of 42 nm in the case of heating at 300°C for 90 min. It was 0.33 at R_p(B) of 61 nm in the case of subsequent heating at 400°C for 30 min. The high activation ratio was achieved by two-step ion implantation method in which boron atoms distributed shallower than argon atoms.

The analysis of experimental results shown from Figs. 2 to 10 clearly shows that Ar precursor implantation is effective to activate boron implanted region. Partially disordered defect states with keeping crystalline states about

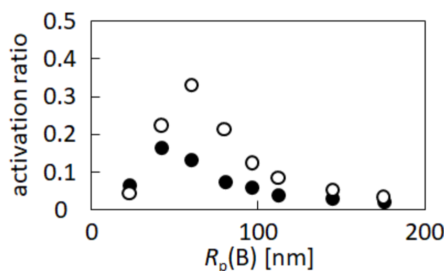

FIGURE 10. Activation ratio as a function of R_p(B) for the 6.0 × 10^{13} cm^{-2} Ar^+ followed by 1.0 × 10^{15} cm^{-2} B^+ two-step-implanted samples heated at 300°C for 90 min (solid circles), and subsequently heated at 400°C for 30 min (open circles).

50% collaboratively formed by the Ar^+ and B^+ implantations is essentially important. Moreover, activation is achieved via reduction of disordered defect states by post heating at low temperature. In the present experimental condition of Ar^+ implantation at 6.0 × 10^{13} cm^{-2} at 70 keV had a peak concentration about 9.0 × 10^{18} cm^{-3} at 80 nm from the surface. The lowest sheet resistivity was given as 392 Ω/sq with R_p(B) of 42 nm in the case of heating at 300°C for 90 min and as 189 Ω/sq with R_p(B) of 61 nm in the case of heating at 400°C for 30 min. The atomic concentrations of Ar in the depth of 42 and 61 nm were 3.2 × 10^{18} and 7.0 × 10^{18} cm^{-3}, respectively. These Ar atomic concentrations ranging 3 × 10^{18} to 7 × 10^{18} cm^{-3} will be a good condition for collaboratively forming the partial disordered region in the boron doped region, which probably causes reduction of the average bonding energy in the silicon lattice system. Moreover, crystalline sites remaining in the doped region will promote effective recrystallization of the disordered states by the post heating. The two-step implantation followed by the post heating has an advantage of activation of boron doped region at low temperature.

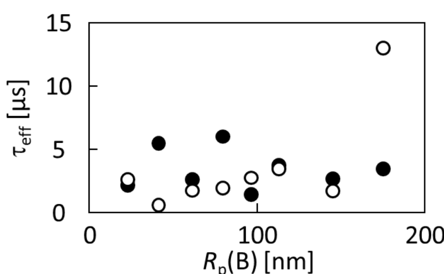

FIGURE 11. τ_{eff} as a function of R_p(B) for the two-step-implanted samples heated at 300°C for 90 min (solid circles), and subsequently heated at 400°C for 30 min (open circles).

On the other hand, there is still a problem for minority carrier. Figure 11 shows τ_{eff} as a function of R_p(B) for the two-step-implanted samples heated at 300°C for 90 min (solid circles), and subsequently heated at 400°C for 30 min (open circles). τ_{eff} was low ranging from 1.3 to 5.9 μs for R_p(B) ranging from 23 to 175 nm in the case of heating at 300°C for 90 min. This indicates that the silicon surfaces had high density of minority carrier recombination defect sites ranging from 2.9 × 10^{12} to 1.3 × 10^{13} cm^{-2} [20]. τ_{eff} was also low values ranging from 0.8 to 3.4 μs for R_p(B) ranging from 23 to 145 nm in the case of heating at 400°C for 30 min. On the other hand, it increased slightly to 13 μs for R_p(B) of 175 nm. The deep boron implantation gave a density of minority carrier recombination defect states of 1.3 × 10^{12} cm^{-2}. These results indicate that Ar^+ implantation caused a high density of minority carrier recombination states. Post heating at 300 and 400°C did not completely reduced the defect states. Passivation technology must be further investigated for formation of doped region with a high activation ratio and a low density of defect states. Moreover, microscopic investigation such as high-resolution secondary ion microscopy will be necessary to make the physics of defect-assisted activation of dopant atoms and criteria of reduction of recombination defect formation [21].

IV. CONCLUSIONS

The two-step ion implantation of Ar^+ and B^+ followed by post annealing was investigated for activating boron implanted region by post heating at low temperatures of 300 and 400°C. The two-step implantation of Ar^+ precursor at 70 keV with the dose ranging from 1.0 × 10^{13} to 5.0 × 10^{14} cm^{-2} followed by B^+ dopant implantation at 20 keV with a dose of 1.0 × 10^{15} cm^{-2} was first investigated. Their projected range was 80 nm. Disordered states were collaboratively formed by Ar^+ precursor followed by B^+ dopant implantation, which decreased X as the Ar dose increased. In the case of an Ar dose of 6.0 × 10^{13} cm^{-2}, X decreased to 0.45 in the boron implanted region and the effective disordered amorphous depth A_{eff} increased to 55 nm. The post heating at 300°C for 90 min followed by 400°C for 30 min effectively recrystallized the boron doped silicon region and decreased A_{eff} to 13 nm. The sheet resistivity also successfully decreased to 302 Ω/sq, whereas it was high of 2400 Ω/sq for the case of the single B^+ implantation at 1.0 × 10^{15} cm^{-2} and 20 keV followed by the post heating. Next, the crystalline state and sheet resistivity were investigated with different projected range of 1.0 × 10^{15}-cm^{-2}-B^+ implantation ranging from 23 to 175 nm given by different acceleration energies ranging from 5 to 50 keV under the condition of 6.0 × 10^{13}-cm^{-2}-Ar^+ precursor implantation at 70 keV (R_P(Ar) = 80 nm). The post heating of 300°C for 90 min followed by 400°C for 30 min was subsequently treated. A_{eff} increased to 61 nm as R_p(B) increased to 100 nm. It gradually decreased as the R_p(B) increased. Although A_{eff} did not decreased to low value by the post heating of 300°C for 90 min followed by 400°C for 30 min when R_p(B) was above 100 nm, it was effectively decreased from 32 (as-implanted) to 1.8 nm by the post heating in the case of R_p(B) of 61 nm. X was decreased to 0.48 in the boron doped region by the two-step implantation in the condition above. Crystalline sites remained as-implanted state would promote recrystallization of the boron doped region by the post heating. The sheet resistivity resonantly decreased to 189 Ω/sq. The activation

ratio was estimated as 0.33 under the assumption of the carrier mobility of 50 cm^2/Vs. We interpret that the high activation ratio was realized via reduction of the average bonding energy in the silicon lattice system by partially introducing disordered states by the two-step implantation and effective recrystallization by the post heating with help of crystalline nucleation sites remained.

However, there is still the problem of the low minority carrier lifetime in the Ar^+ and B^+ two-step implantation system. Although the majority carriers were effectively generated via activation of the present two-step implantation method, we estimated that the density of recombination defect states still remained in the doped region. Defect passivation should be further investigation for example additional hydrogenation.

REFERENCES

[1] S. Uchikoga and N. Ibaraki, "Low temperature poly-Si TFT-LCD by excimer laser anneal," *Thin Solid Films*, vol. 383, nos. 1–2, pp. 19–24, Feb. 2001, doi: 10.1016/S0040-6090(00)01644-8.

[2] S. Inoue, K. Sadao, T. Ozawa, Y. Kobashi, H. Kwai, T. Kitagawa, and T. Shimoda, "Low temperature poly-Si TFT-electrophoretic displays (TFT-EPDs) with four level gray scale," in *IEDM Tech. Dig.*, Dec. 2000, pp. 197–200, Dec. 2000, doi: 10.1109/IEDM.2000.904291.

[3] T. Sameshima, S. Usui, and M. Sekiya, "XeCl excimer laser annealing used in the fabrication of poly-Si TFT's," *IEEE Electron Device Lett.*, vol. 7, no. 5, pp. 276–278, May 1986, doi: 10.1109/EDL.1986.26372.

[4] M. A. Green, "Commercial progress and challenges for photovoltaics," *Nature Energy*, vol. 1, no. 1, Jan. 2016, Art. no. 15015.

[5] M. Dahlinger, B. Bazer-Bachi, T. C. Röder, J. R. Köhler, R. Zapf-Gottwick, and J. H. Werner, "22.0% efficient laser doped back contact solar cells," *Energy Procedia*, vol. 38, pp. 250–253, Sep. 2013.

[6] M. Mehrotra, J. C. Hu, and M. Rodder, "A 1.2 V, sub-0.09 μm gate length CMOS technology," in *IEDM Tech. Dig.*, Dec. 1999, pp. 419–422, doi: 10.1109/IEDM.1999.824183.

[7] T. Ito, K. Suguro, M. Tamura, T. Taniguchi, Y. Ushiku, T. Iinuma, T. Itani, M. Yoshioka, T. Owada, Y. Imaoka, H. Murayama, and T. Kusuda, "Flash lamp annealing technology for ultra-shallow junction formation," in *Proc. Extended Abstr. 3rd Int. Workshop Junction Technol. (IWJT)*, Dec. 2002, pp. 23–26, doi: 10.1109/IWJT.2002.1225191.

[8] A. Shima and A. Hiraiwa, "Ultra-shallow junction formation by non-melt laser spike annealing and its application to complementary metal oxide semiconductor devices in 65-nm node," *Jpn. J. Appl. Phys.*, vol. 45, no. 7, pp. 5708–5715, Jul. 2006, doi: 10.1143/JJAP.45.5708.

[9] K. Goto, T. Yamamoto, T. Kubo, M. Kase, Y. Wang, T. Lin, S. Talwar, and T. Sugii, "Ultra-low contact resistance for deca-nm MOSFETs by laser annealing," in *IEDM Tech. Dig.*, Dec. 1999, pp. 931–933, doi: 10.1109/IEDM.1999.824302.

[10] H. Onoda, Y. Nakashima, T. Nagayama, and S. Sakai, "High dose dopant implantation to heated Si substrate without amorphous layer formation," in *Proc. 13th Int. Workshop Junction Technol. (IWJT)*, Jun. 2013, pp. 66–69.

[11] T. Nagao, T. Uehara, K. Yasuta, Y. Inouchi, J. Tatemichi, M. Hasumi, and T. Sameshima, "Two-step ion implantation used for activating boron atoms in silicon at 300 °C," in *Proc. 25th Int. Workshop Active Matrix Flatpanel Display Devices*, Sep. 2018, pp. 1–4.

[12] J. F. Ziegler and J. M. Manoyan, "The stopping of ions in compounds," *Nucl. Instrum. Methods*, vol. B35, pp. 215–228, Dec. 1988.

[13] M. Born and E. Wolf, *Principles of Optics*. New York, NY, USA: Pergamon, 1974, ch. 1, p. 13.

[14] K. Ukawa, Y. Kanda, T. Sameshima, N. Sano, M. Naito, and N. Hamamoto, "Activation of silicon implanted with phosphorus and boron atoms by infrared semiconductor laser rapid annealing," *Jpn. J. Appl. Phys.*, vol. 49, no. 7, Jul. 2010, Art. no. 076503.

[15] T. Sameshima, H. Hayasaka, and T. Haba, "Analysis of microwave absorption caused by free carriers in silicon," *Jpn. J. Appl. Phys.*, vol. 48, no. 2, Feb. 2009, Art. no. 021204.

[16] T. Sameshima, T. Motoki, K. Yasuda, T. Nakamura, M. Hasumi, and T. Mizuno, "Photoinduced carrier annihilation in silicon pn junction," *Jpn. J. Appl. Phys.*, vol. 54, no. 8, Aug. 2015, Art. no. 081302.

[17] H. Engstrom, "Infrared reflectivity and transmissivity of boron-implanted, laser-annealed silicon," *J. Appl. Phys.*, vol. 51, no. 10, pp. 5245–5249, 1980, doi: 10.1063/1.327476.

[18] T. Sameshima, K. Yasuta, M. Hasumi, T. Nagao, and Y. Inouchi, "Activation of dopant in silicon by ion implantation under heating sample at 200 ◦C," *Appl. Phys. A, Solids Surf.*, vol. 124, no. 3, p. 228, Mar. 2018.

[19] Y. Taur and T, Ning, *Fundamental of Modern VLSI Physics*. Cambridge, U.K.: Cambridge Univ. Press, 1998, ch. 2. p. 20.

[20] D. J. Fitzgerald, "Radiation-induced increase in surface recombination velocity of thermally oxidized silicon structures," *Proc. IEEE*, vol. 54, no. 11, pp. 1601–1602, Dec. 1966, doi: 10.1109/PROC.1966.5217.

[21] A. K. W. Chee, "Principles of site-selective doping contrast in the dual-beam focused ion beam/scanning electron microscope," *Ultramicroscopy*, Jan. 2020, Art. no. 112947, doi: 10.1016/j.ultramic.2020.112947.

TOSHIYUKI SAMESHIMA received the M.E. and D.E. degrees from the Department of Science, Shizuoka University, Shizuoka, Japan, in 1980 and 1991, respectively. He is currently a Professor with the Department of Electrical and Electronics Engineering, TUAT, and a member of the Japan Society of Applied Physics. He published 153 refereed original articles and 112 patents. His research interests include semiconductor device, processing technology, and evaluation analysis.

TOMOKAZU NAGAO received the M.E. degree from the Department of Electrical and Electronics Engineering, Tokyo University of Agriculture and Technology, Japan, in 2012. In 2012, he joined Nissin Ion Equipment Company, Ltd., Kyoto, Japan, where he has been engaged in ion implantation technology and development of ion implanter.

ERIKA SEKIGUCHI is currently pursuing the degree with the Department of Electrical and Electronics Engineering, Tokyo University of Agriculture and Technology, Tokyo, Japan. Her research interests include the two-step ion implantations process and thesis.

MASAHIKO HASUMI received the Ph.D. degree from the Graduate School of Arts and Science, University of Tokyo, Japan, in 1992. He is currently an Assistant Professor with the Department of Electrical and Electronics Engineering, TUAT, Japan, and a member of the Japan Society of Applied Physics and the Physical Society of Japan. He published 40 refereed original articles. His research interests include semiconductor devices, processing technology, and evaluation analysis.